Thermomechanical modeling of extensional gneiss domes

Céline Tirel
Géosciences Rennes UMR 6118 CNRS, Université de Rennes 1, Rennes, France. celine.tirel@univ-rennes1.fr

Jean-Pierre Brun
Géosciences Rennes UMR 6118 CNRS, Université de Rennes 1, Rennes, France.

Evgenii Burov
Laboratoire de Tectonique UMR 7072 CNRS, Université Pierre et Marie Curie, Paris, France

Publié sous la référence:
Tirel, C., Brun, J.-P., and Burov, E., 2004, Thermomechanical modeling of extensional gneiss domes, *in* Whitney, D.L, Teyssier, C., and Siddoway, C.S., Gneiss domes in orogeny: Boulder, Colorado, Book Series: Geological Society of America Special Papers, Volume: 380, p. 67-78. ISSN: 0072-1077; ISBN: 978-0-8137-2380-8

Abstract

We use a thermo-mechanical modeling approach to study the development of extensional gneiss domes in a thickened and thermally relaxed lithosphere. Our models consider a compositional and thermally dependent rheological lithosphere layering, with a 60 km thick crust and Moho temperatures in the range 840-1040 °C. No discontinuity or detachment fault is assumed to preexist within the upper crust. However, to initiate localized deformation, a density anomaly is placed at the base of middle crust. Extension is applied to one model boundary at constant rates of 2.0 and 0.66 cm/y. Models illustrate the progressive development of domes and associated strain patterns at crustal scale. Extension first localizes in the upper crust as a nearly symmetrical graben, allowing the underlying middle and lower ductile crust to rise up, initiating a dome. Dome amplification is further accommodated by convergent channel flow in the lower crust. Strain localization displays a complex pattern of shear zones at the crustal scale, first nearly symmetrical, and progressively becoming asymmetrical, giving, in particular, an upward convex detachment on one side of the dome. During extension, Moho geometry and depth vary as a function of boundary displacement rate. At the lower boundary displacement rate used in the calculations, the Moho remains rather flat and rises up at a constant rate. Results are discussed in the light of field examples and compared to previous models.

2.1. Introduction

Gneiss domes are common features of orogenic belts and their origin has long been debated between diapirism (e.g. Ramberg (1981)) or superposed folding (e.g. Ramsay (1967)). The identification, in the Basin and Range of the Western US, of extensional detachment faults associated with core complexes (Crittenden et al., 1980; Davis and Coney, 1979; Wernicke, 1981; Wernicke, 1985) has been a major breakthrough, adding crustal extension as a new important mechanism for the origin of gneiss domes. Similar structures, closely related to gneiss domes, were later found in the Aegean and Thyrrhenian Sea (Gautier et al., 1990; 1993; Jolivet et al., 1998; Lister et al., 1984) and in older orogens (Andersen et al., 1991; Burg et al., 1994; Echtler and Malavieille, 1990; Malavieille et al., 1990; Norton, 1986; Seranne and Seguret, 1987; Van Den Driessche and Brun, 1989; Van Den Driessche and Brun, 1991). As in the Basin and Range (Coney and Harms, 1984), extensional gneiss domes appeared to be symptomatic features of lithosphere-scale extension following crustal thickening. Whereas the mechanics of detachment faults has long been a matter of debate (Brun et al., 1994; 1995; Buck, 1988; Lavier et al., 1999; Lavier et al., 2000; Lister and Davis, 1989; Scott and Lister, 1995; Spencer, 1984; Wernicke, 1981; 1985; Wernicke and Axen, 1988), the structure and development of metamorphic domes in detachment footwalls has attracted rather little attention. However, Block and Royden (1990) and Buck (1991) pointed out that the so-called “core complex mode” requires a lower crust viscosity low enough to flow rapidly, allowing the surface and Moho to remain relatively flat during dome rise and continuing extension.

In the present paper, we use thermo-mechanical crustal-scale and lithosphere-scale models to study the initiation and deformation patterns of extensional gneiss domes. Models simulate the asymmetric extension of a “hot lithosphere” with a 60 km thick crust and Moho temperatures in the range 840-1040°C. We do not-introduce any pre-existing faults in the upper crust, but a small density anomaly mimicking a granitic inclusion is imposed at the base of the middle crust, to initiate localized deformation. Results illustrate initial necking of the upper crust, dome shape evolution, channel flow in the lower crust and patterns of shear zones at the crustal scale. The influence of boundary displacement rate on dome amplification, deformation patterns and Moho geometry is discussed.

2.2. Tectonic setting and structure of extensional gneiss domes

More than a hundred years of field studies have documented that mountain building is accompanied by temperature rise, which is responsible for metamorphism, partial melting and ductile flow of crustal rocks. Numerical modeling of thermal relaxation induced by crustal thickening indicates that Moho temperatures can reach the range 800-1000°C at depths of 50-60 km (England and Richardson, 1977; England and Thompson, 1986; Oxburg and Turcotte, 1974). In addition, in large mountain belts where thickening is maintained long enough, other phenomena can contribute to increasing of crustal temperature. In particular, magmas derived from mantle can be emplaced in the lower crust. The lithospheric mantle can undergo delamination (Bird, 1979) or thermo-mechanical erosion by small-scale convection (Doin and Fleitout, 1996).

For Moho temperatures higher than 700°C, lithosphere strength is reduced to a degree such that gravitational collapse is likely to occur (England and Bickle, 1984; Gaudemer et al., 1988; Ranalli, 1997; Sonder et al., 1987). Gravitational collapse and related

crustal extension (Rey et al., 2001) occurred in most orogens of Alpine age (Dewey, 1988) as well as in older Phanerozoic ones (Andersen et al., 1991; Burg et al., 1994). Extension is not restricted to those domains of thickened crust undergoing post-thickening divergent displacement at one of their boundaries (Gautier et al., 1999; Oldow et al., 1989). It can also develop during convergence, at the borders of thickened domains (Burg et al., 1984; Herren, 1987; Royden and Burchfield, 1987), or within thickened domains due to lateral extrusion (Armijo et al., 1986; Ratschbacher et al., 1989). The Hercynian belt of Western Europe provides an example of gravity collapse induced extension during and after convergence (Burg et al., 1994; Van Den Driessche and Brun, 1991).

Extensional gneiss domes and/or core complexes have been identified and described in all the tectonic settings mentioned above. For the purpose of the present paper, we focus on extensional gneiss domes developing after crustal thickening. However, a number of the structural features developed put forward here could apply to other types of tectonic settings.

The main structural features of an extensional gneiss dome are here summarized following Brun and Van Den Driessche (1994) (Fig. 2-1A). The overall structure has a characteristic transverse size of some tens of kilometers. The dome core, made of metamorphic rocks migmatites and granite bodies, is surrounded by upper crustal units and sediments deposited during dome formation. Due to the presence of a detachment fault, the internal structure is more generally asymmetric but this is not necessarily a rule. If the dome core is lighter than the surrounding rocks – i.e., granites or migmatites- a diapiric component can participate in the dome rise, leading to more symmetrical deformation patterns. For the purpose of the present paper we, however, concentrate on those domes which display a clear asymmetry. Below the flat lying part of the detachment, the footwall can display a broad upward bending. Consequently and after erosion, an upper to middle crust section can be exposed with the deeper levels close to the detachment (see surface of the 3D diagram fig.2-1A). The detachment hanging-wall is a section of upper crust brought in direct contact with deep core (mid- to lower crustal) rocks by the detachment. The detachment geometry is most often convex upward, with a flat-lying part on the dome's top and a more steeply dipping part along one dome limb. Sediments deposited during dome formation are generally affected by normal faulting above the detachment. Thick depocenters can be observed close to the steeper part of the detachment and sediments deposited at early stages of dome deformation are commonly strongly tilted within small fault blocks lying on top of the flat part of the detachment.

Within the metamorphic core, the dome shaped foliation envelope (Fig. 2-1B) is associated with opposite senses of shear along opposite dome limbs. However, finite strain intensities are higher in the detachment zone, as demonstrated by the common presence of C/S mylonites (according to Berthé et al., 1979). Because of the opposite senses of shear, a zone of co-axial incremental strain is expected to occur in the central part of the dome. This deformation pattern suggests that ductile material flows laterally into the dome, from below, through lower crustal channels.

Due to cooling during dome rise, the brittle-ductile transition migrates downward with respect to the exhuming dome. Consequently, rocks that were previously ductile become brittle as observed in most extensional gneiss domes that exhibit complex superposition of brittle deformation on ductile fabrics. In the detachment zone, high temperature mylonites are commonly reworked by cataclasites and breccias. Within the rest of the dome, faults and associated brittle features are superposed on metamorphic foliations, ductile shear zones, folds, and boudinage. At map scale, metamorphic isograds are generally folded together with

the dome foliation and are cut by the detachment zone. Apparent temperature gradients calculated from the distance separating metamorphic isograds are often extremely high (i.e. commonly more than 100°C/km), indicating strong shortening parallel to the pre-existing metamorphic layering.

In post-convergence settings, another important feature observed at the crustal scale in the Basin and Range (Allmendinger et al., 1987; Hauser et al., 1987) and the Aegean (Makris, 1978; Sachpazi et al., 1997) is the flat geometry of the Moho below extensional gneiss domes. As argued by Block and Royden (1990), Buck (1991) and, more recently, by McKenzie et al. (2000) this requires lower crustal flow at the regional-scale, driven by lateral pressure gradients caused by differential thinning of the overlying crust. It is also interesting, for the purpose of our modeling, to note that in both the Basin and Range and Aegean, extension results from the displacement of one boundary of the previously thickened domain, with mean displacement rates lower than 2 cm/y.

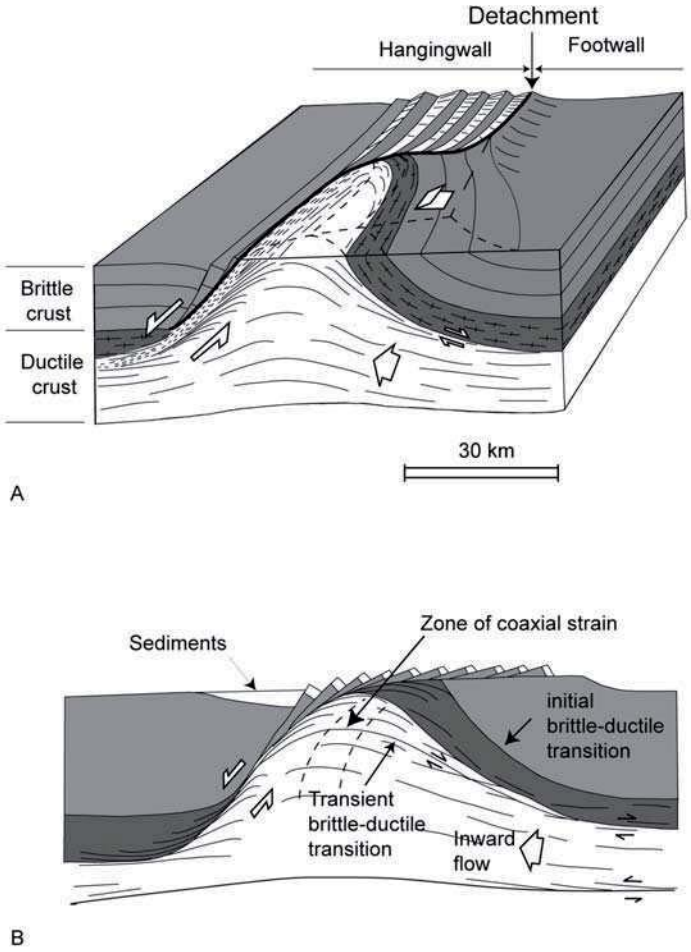

Figure 2-1: *Three-dimensional structure of extensional gneiss domes (A) and kinematic and strain pattern (B) (Modified after Brun and Van Den Driessche, 1994). The sedimentary basin with normal faulting in the detachment hanging wall is not shown*

2.3. Numerical modeling

2.3.1. Rheology, initial and boundary conditions

The model setup is shown in Figure 2-2. Lithosphere models have spatial dimensions of 400 km x 100 km and numerical grid dimensions of 200 x 50 quadrilateral bilinear elements (2 km x 2 km) each element being subdivided in the two pairs of triangular sub-elements (4000 triangular sub-elements). The thickened continental crust has a pre-collapse thickness of 60 km, which corresponds to a typical Alpine orogenic belt. Horizontal displacement was applied at the left boundary of the model at rates of 0.66 cm/y and 2.0 cm/y. The model surface is free and the bottom boundary condition is represented by a pliable Winkler basement, which implies vertical normal stresses proportional to vertical displacement of the boundary multiplied by the density contrast (Burov and Cloetingh, 1997). For the initial thermal field, we use two conductive geotherms G_1 and G_2 yielding initial Moho temperatures of 1040°C and 840°C, respectively. The surface temperature is fixed at 0°C and zero heat flux is used as the lateral boundary condition.

The continental crust has an average quartz diorite-type composition, with a density of 2800 kg/m^3. The crust is arbitrarily divided into three marker layers that represent upper, middle and lower crust. The latter is divided into two sub-layers with different colours, for a better visual tracing of the developing structures. The lithospheric mantle is composed of olivine with a density of 3300 kg/m^3.

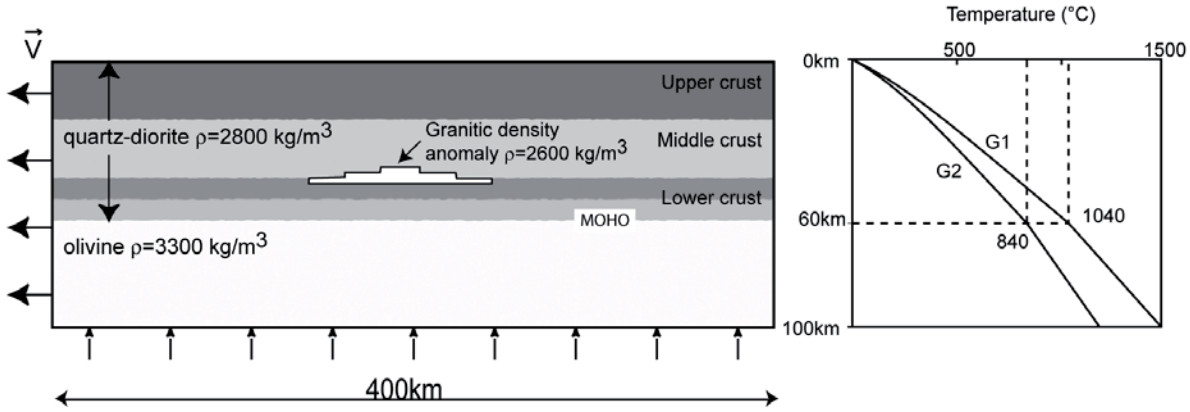

Figure 2-2: *Model geometry, velocity boundary conditions, and initial geotherms with Moho temperatures at 60 km depth. Model parameters are summarized in Table 2-1. Note the presence of a density anomaly at base of the middle crust at the model center*

The rheology of the materials in the model is non-linear, brittle-elasto-ductile. The material parameters for ductile creep come from Ranalli and Murphy (1987) for the quartz diorite, Kirby and Kronenberg (1987) for the granite inclusion, and Brace and Kohlstedt (1980) for olivine (Table 2-1). Ductile creep is described by a power law relationship between strain rate and stress (Kirby and Kronenberg, 1987):

$$\dot{\varepsilon} = A_0(\sigma_1 - \sigma_3)^n \exp(-H/RT)\,, \qquad (1)$$

where $\dot{\varepsilon}$ is the strain rate, *T* the temperature, σ_1 and σ_3 the principal stresses, and A_0, *H*, *R*, and *n* are material constants (Table 2-1).

The brittle rheological term is approximated by Mohr-Coulomb plasticity with a friction angle of 30° and a cohesion of 20 MPa (Gerbault et al., 1999). The values for the elastic moduli are *E* = 80 GPa and υ = 0.25 (Young's modulus and Poisson coefficient, respectively (Turcotte and Schubert, 1982)).

Except for variations in boundary displacement rates (V_1= 0.66 cm/y and V_2 = 2.0 cm/y) and of the initial geotherms (G_1 and G_2, Fig. 2-2), all other parameters of the models presented here remained unchanged through all experiments.

The absence of lateral heterogeneities of viscosity or density in the middle-lower crustal part of the models gives a uniform extension with no local thinning of the upper brittle layer. The same conclusion was gained by Brun et al. (1994) using analogue models. We therefore introduced in the center of the model, close to the middle-lower crust interface (Fig. 2-2), a low density (2600 kg/m^3) triangle shaped heterogeneity, mimicking a conical intrusion.

Different shapes and sizes of the heterogeneity have been tested that give no significant differences in the final result. For the purpose of the present paper, the size of the heterogeneity is 4 km in height and 80 km in width. In nature this should correspond to laccolith type granite bodies (Roman-Berdiel et al., 1995) comparable in size and composition to those directly observed in the Himalayas (e.g. Lefort et al., 1987; Scaillet et al., 1995). It will be seen further in the paper that during the formation of an extensional gneiss dome the heterogeneity is extremely deformed leading to a sill-like body bended around the external part of the dome. Such strongly deformed sills of granites with C/S mylonite fabrics are often observed in close connection with detachment zones within the extensional gneiss domes (Gautier and Brun, 1994b; Gautier et al., 1993; Rehrig and Reynolds, 1980; Reynolds and Rehrig, 1980; Van Den Driessche and Brun, 1991). Moreover, Lister and Baldwin (1993) suggested that the formation of metamorphic core complexes may be triggered by plutonic activity during episodes of continental extension. It is finally interesting to note that a number of conceptual models of gneiss dome formation also postulate the presence of laccolith or sill granitic bodies in the middle of the crust, prior to dome development (e.g. see fig. 8 of Norlander et al. (2002).

Crustal thickening induced metamorphism which likely precedes large scale extension like in the Basin and Range or the Aegean may enhance the lowering of crustal density with depth. As argued by Gerya et al. (2001), this can lead to gravitational instability due to changes in mineral assemblages and the thermal expansion of minerals. Such density changes and related buoyancy effects have not been taken into account in the calculations presented here, except for the local anomaly placed at the center of the models. We are

convinced of the importance of buoyancy but our purpose is primarily to study here the process of gneiss dome exhumation in absence of any diapiric effect. Further calculations will consider situations in which diapirism interacts with extension and their potential application to natural examples (e.g. Vanderhaeghe et al. 1999).

Variables/Parameters	Values and Units	Comments
Initial crustal thickness	60×10^3 m	Continental crust
Initial upper crust thickness	22×10^3 m	Continental crust
Initial middle crust thickness	22×10^3 m	Continental crust
Initial lower crust thickness	16×10^3 m	Continental crust
Extension rate	0.66 $cm.y^{-1}$, 2 $cm.y^{-1}$	Applied on left side
Initial Moho temperature	840°C, 1040°C	Applied geotherms
Power law constant A_1	1.26×10^{-3} $MPa^{-n}.s^{-1}$	Quartz-diorite (crust)
Power law constant n_1	2.4	Quartz-diorite (crust)
Creep activation enthalpy H_1	219 $kJ.mol^{-1}$	Quartz-diorite (crust)
Power law constant A_2	1.25×10^{-9} $MPa^{-n}.s^{-1}$	Granite (anomaly)
Power law constant n_2	3.2	Granite (anomaly)
Creep activation enthalpy H_2	123 $kJ.mol^{-1}$	Granite (anomaly)
Power low constant A_3	7×10^4 $MPa^{-n}.s^{-1}$	Olivine (mantle)
Power law constant n_3	3	Olivine (mantle)
Creep activation enthalpy H_3	520 $kJ.mol^{-1}$	Olivine (mantle)
Density ρ_1	2800 $kg.m^{-3}$	Crust
Density ρ_2	2600 $kg.m^{-3}$	Anomaly of granite
Density ρ_3	3300 $kg.m^{-3}$	Mantle
Thermal conductivity k_1	2.5 $W.m^{-1}.K^{-1}$	Crust
Thermal conductivity k_2	3.3 $W.m^{-1}.K^{-1}$	Mantle

Table 2-1: *Parameters used in models*

2.3.2. Thermomechanical model

The large-strain thermo-mechanical code PAROVOZ (Poliakov et al., 1993) used for our computations is a hybrid finite element/finite differences, fully explicit, time-marching Lagrangian algorithm, derived from the algorithm used in *FLAC*® (Cundall, 1989). This widely used algorithm was described in detail in several previous studies (Cundall, 1989; Poliakov et al., 1993; Lavier et al., 2000; Burov and Poliakov, 2001). We therefore limit the description of the code to explanations of its basic features.

The code solves equilibrium problems for brittle-elasto-ductile media using general Newtonian law equations of motion in the continuum mechanics formulation:

$$\frac{\rho \partial v_i}{\partial t} - \frac{\partial \sigma_{ij}}{\partial x_j} - \rho g_i = 0 , \qquad (2)$$

where v is velocity, ρ is P-T independent density, t is time, g is acceleration due to gravity, and σ is stress.

This method allows the use of a small strain formulation for large strain problems because the Lagrangian mesh moves and deforms with the material. At each time step, the new positions of the mesh grid nodes are calculated from the current velocity field and updated in large strain mode accounting for rotation of principal stress axes. Solutions for velocities at mesh points are used to calculate element strains ε_{ij} that are employed in the constitutive relations yielding element stresses σ_{ij} and forces $\rho \partial v_i / \partial t$. The latter provide input for the next step of calculation. In quasi-static mode, the algorithm uses artificial inertial masses to suppress inertial effects (Cundall, 1989).

The mechanical and constitutive equations are coupled with the heat transport equations:

$$div(\mathbf{k} \nabla T) - \rho C_p \frac{\partial T}{\partial t} + H_r = \mathbf{v} \nabla T , \qquad (3)$$

where $\mathbf{v}$ is the velocity vector, C_p is the specific heat, k is the thermal conductivity, H_r is the heat production (radiogenic and frictional dissipation) per unit volume (Table 1).

The right side of the Equation (3) is calculated directly from solutions of Equation (2), while the left side is computed using a separate numerical scheme. A dynamic relaxation technique, based on the introduction of artificial inertial masses in the dynamic system, is used to allow for explicit solution of the governing Equation (2).

An important feature of the method relates to its capacity to handle nonlinear temperature, stress and strain rate dependent rheologies and, specifically, to its capability to localize non-predefined brittle faulting (Cundall, 1990; Lavier et al., 2000). The other important feature of this method is that the code is fully thermally coupled and that each grid element simultaneously includes all three rheological terms, brittle, elastic and ductile. Thus the local deformation mode may change from brittle to ductile or elastic, depending on mechanical and temperature conditions.

2.4. Results

For the purpose of the present paper, we here concentrate on results directly relevant to the development and structure of extensional gneiss domes. The initial Moho temperature (T_{moho}) and the applied boundary displacement rates (V_{ext}) have direct influence on dome amplification rate and decrease in Moho depth during extension. The deformation history of all models can be divided into two successive stages, here called “upper crust necking” and “dome amplification”. Taking a 40 km depth as the reference level, the dome amplification curves show that, after a stage during which the upper crust undergoes a necking instability, amplification is a rather linear function of time and V_{ext} (Fig. 2-3). Moho depth curves display two different types of behavior. At V_1= 0.66 cm/y, they also show a linear dependence with time; for G_2 at V_2= 2.0 cm/y they tend to temporarily stabilize around 40 km. The comparison of dome amplification and decrease in Moho depth shows that, in the range of explored values, the influence of variations in V_{ext} is stronger than that of T_{moho}.

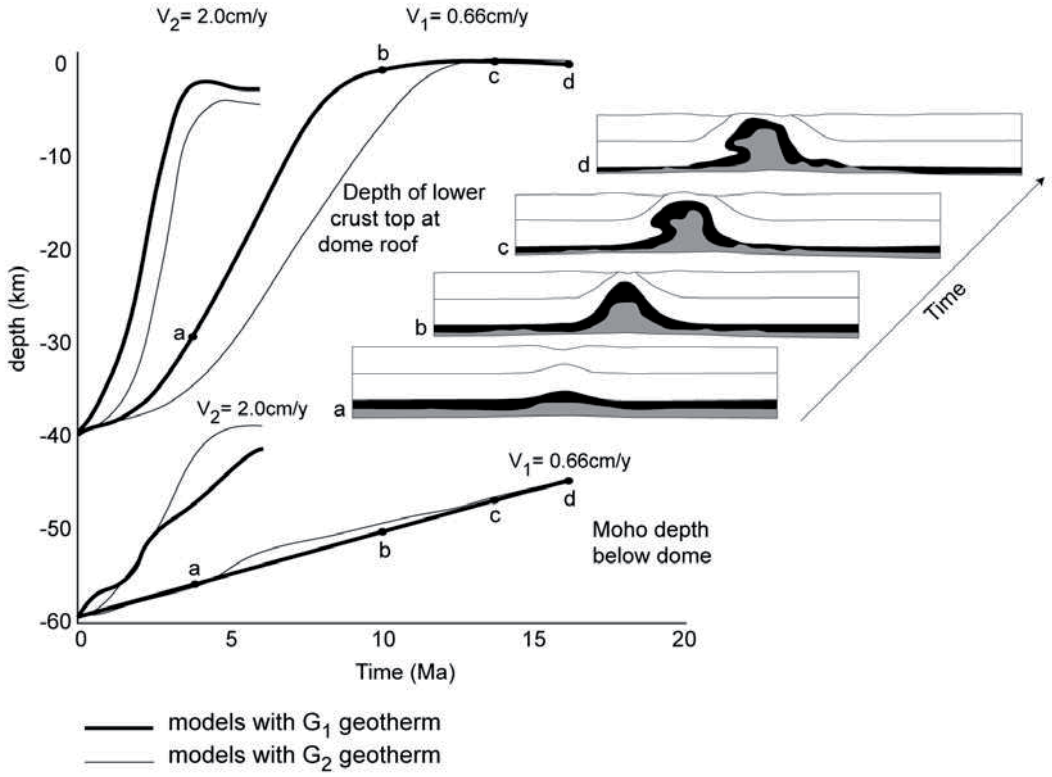

Figure 2-3: *Dome amplification and Moho rise as functions of time for boundary displacement rates V_1 = 2.0 and V_2 = 0.66 cm/y and initial geotherms G_1 and G_2 with Moho temperatures T_{M1} =1040 and T_{M2} = 840°C respectively. A time series of sections show the dome shape evolution for V_1 = 0.66 cm/y and T_{M1} =1040°C with reference to the corresponding curves of dome amplification and Moho rise. Section (a) corresponds to the necking stage of upper brittle crust. Sections (b) to (d) illustrate stages of dome amplification.*

Comparison of four models (Fig. 2-4) for different combinations of T_{moho} and V_{ext} shows shapes of domes and of 400-600°C isotherms, but significant variations in Moho geometry. Moho arching below the dome tends to increase with V_{ext} and to decrease with T_{moho}. Figure 2-4 also shows that within the domes, the middle and lower crustal interfaces are strongly advected towards the surface, so that they are found above the 400°C and 600°C isotherms. Since the ductile-brittle transition occurs at temperatures close to 400°C, the upper part of domes becomes brittle and mechanically integrated into the upper brittle crust. Similar effects are observed in models of magma chamber emplacement (Guillou-Frottier et al., 2000).

All experiments display a number of similar features for the whole range of variation of input parameters. This relates, in particular, to the progressive evolution of dome shape and of the pattern of total shear strain intensity that are illustrated using the model with initial Moho temperature of 1040°C (geotherm G_1) and a boundary displacement rate V_1= 0.66 cm/y (Fig. 5).

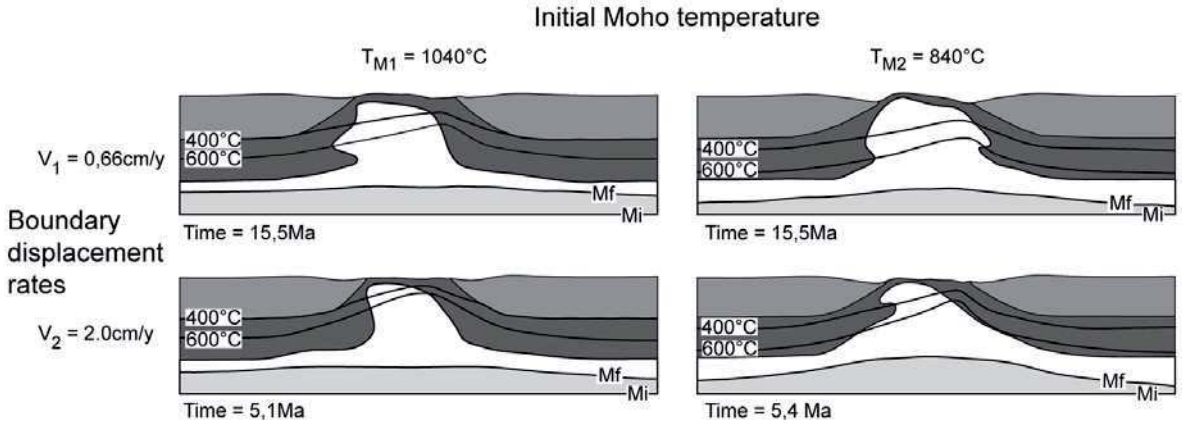

Figure 2-4: *Shapes of domes and 400 – 600°C isotherms for boundary displacement rates V_1 = 2.0 and V_2 = 0.66 cm/y and initial Moho temperatures T_{M1} =1040 and T_{M2} = 840°C.*

2.4.1. Upper crust necking stage

At an early stage of extension (4 Ma; Fig. 2-5A), the upper crust undergoes a necking instability above the density heterogeneity. Strain rates, not shown here, show that necking is accommodated by steep conjugate normal faults, defining a symmetrical graben (Figs. 2-5A,B). On both graben sides, the upper crust remains mostly undeformed. The upward bending of middle and lower crust, below the upper crust neck, corresponds to the future dome. Variations in total shear strain intensity (4 Ma; Figs. 2-5B,C) display an upper central zone of deformation that corresponds to the graben and underlies deformed middle and lower crust. It is bounded by flat lying zones of deformation located in the lower crust. Contours of total shear strain intensities reveal a pattern of flat lying shear zones with conjugate senses of shear (Fig.2-6A) that results from channel flow in the lower crust. Highest strain intensity shear zones are located at the base of the middle crust with divergent

senses of shear – i.e., top away from the central zone. Two other shear zones are located at the base of lower crust with convergent senses of shear – i.e., top to the central zone. Even at this early stage of extension, a slight asymmetry is already present in the shear zone pattern, with one of the basal lower crust shear zones bending upward below the upper crust neck (Fig. 2-6).

2.4.2. Dome amplification stage

During the second stage, the dome amplifies rapidly and the upper crust undergoes extreme thinning and rupture. The dome shape becomes rapidly asymmetrical (Figs. 2-5A, 2-6). At 10 Ma, the middle crust reaches the surface. Between 10 and 16 Ma, the lower crustal layer rises nearly vertically in the dome core. During the rise of lower crust, the middle crust undergoes layer parallel shearing, with opposite senses of shear on right and left dome limbs, and strong layer perpendicular shortening (Fig. 2-6). Variations in total shear strain intensity (Fig. 2-5B) show the evolution of the shear zone pattern. At 10 Ma, basal middle crust shear zones bend upward with the one opposite to the moving boundary reaching the surface. Between 10 and 16 Ma the shear zone pattern becomes strongly asymmetric. The middle crust shear zone, forming the right dome limb, is the major zone of localized displacement at model scale – i.e., it is an extensional detachment.

At mature stages of dome growth, the detachment zone displays a sigmoid shape made of three main parts: flat at the dome top, steeply dipping along the dome limb, and flat again in the middle crust. Successive total shear strain sections (Fig. 2-5B) illustrate the way this complex detachment zone develops. At “upper crustal necking stage” no detachment is present (Fig. 2-6A). By 10Ma a connection is almost achieved, between a zone of high strain intensity located at graben base and a basal middle crust shear zone (Figs. 2-5C and 2-6A), which gives birth to the detachment. The shear zone located along the opposite dome limb is nearly connected to the surface at 10 Ma. Further stages of evolution show that this shear zone reduces in width to become localized in the middle crust (14 and 16 Ma in Figs. 2-5B, D), suggesting that its development is inhibited by the detachment.

Instantaneous velocity fields have been plotted on enlarged sections of total shear strain intensity for the “upper crust necking” and “mature dome” stages (Figs. 2-5C, D). Comparison between the two stages of evolution shows that there is no strong change in the overall velocity pattern during model evolution except in the lower crust and mantle, in the left part of the model. In both sections, the upper crust and a part of middle crust do not move at all or displace horizontally as rigid blocks. Long and steeply inclined vectors are located below the graben zone, at the necking stage (Fig. 2-5C), and in the right part of the dome, at the mature dome stage (Fig. 2-5D). Horizontal or nearly horizontal vectors with large magnitude, in the left half of the mature dome (Fig. 2-5D), result from incorporation in the upper brittle crust of the previously ductile middle and lower crustal material. The change of vector inclination, from steeply inclined close to the detachment to nearly horizontal in the opposite half of the dome, highlights the asymmetry of dome growth.

The lower crust and underlying mantle display two types of velocity patterns. To the right, vectors are nearly horizontal with magnitude increasing downward, at both necking and mature stages. To the left, vectors are directed to the right and left at necking and mature stages, respectively. In both cases, their magnitude decreases downward. As a whole, the velocity fields illustrate the kinematic relationships between channel flow in the lower crust and dome amplification.

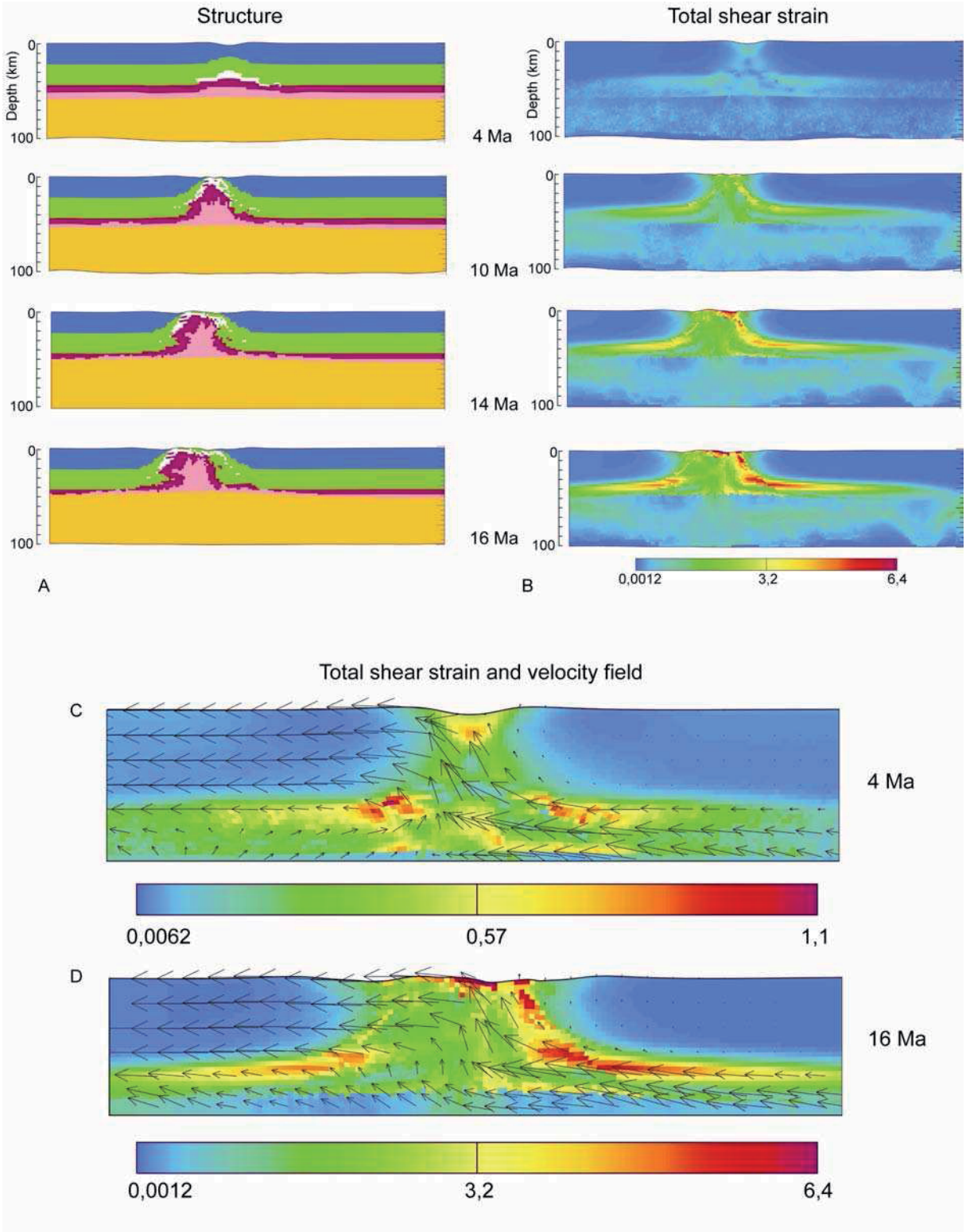

Figure 2-5: *Structure (A) and total shear strain (B) of model with boundary displacement rate V_1= 0.66 cm/y and initial Moho temperature T_{M1} =1040°C (geotherm G_1). Stages of evolution, given in Ma, illustrate the stages of "upper crust necking" (4 Ma) and "dome amplification" (From 10 to 16 Ma). Enlargements of total shear strain patterns with superposed instantaneous velocity fields correspond to the "upper crust necking" stage at 4 Ma (C) and a mature dome at 16 Ma during the course of "dome amplification" (D). In (C) the scale of strain intensity has been adapted to better reveal strain intensity variations.*

In all models, an overhang develops in the dome limb opposite to the detachment, adding to the overall dome asymmetry (Fig. 2-6B). This particular feature displays a close geometrical relationship with the flat lying shear zone located in the middle crust (Fig. 2-5D). Above the shear zone, the upper part of the dome is transported laterally, away for the detachment (Fig. 2-5D). Below the shear zone, the lower crust flows towards the dome. As a result, the dome limb is progressively distorted at the tip of the shear zone forming an overhang at middle crust level. Interestingly, comparable overhang structures appear in Wdowinsky and Axen (1992)'s models (see their fig. 6c). In their models, like in ours, such structures are directly related to inward flow of lower crust in the dome base, opposite to the detachment zone.

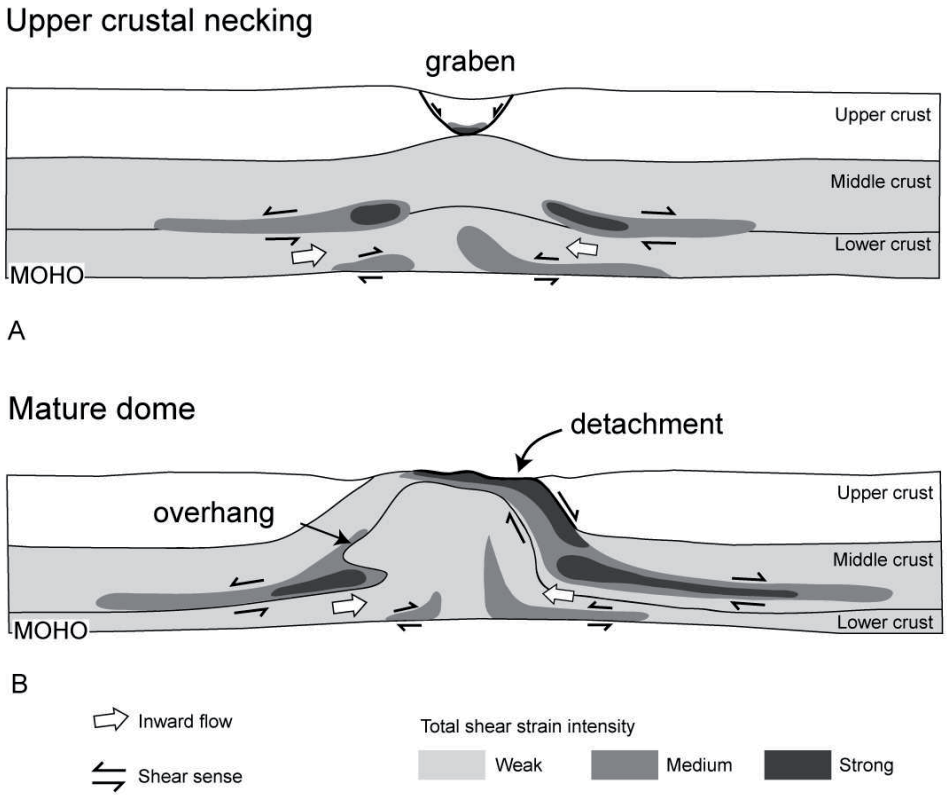

Figure 2-6. *Shear zone patterns associated with extensional gneiss dome evolution at the crustal scale. At upper crust necking stage (A), crustal scale deformation is close to pure shear with a symmetrical graben in the upper crust and a symmetrical pattern of shear zones, associated with lower crustal flow, with opposite senses of shear. At the mature dome stage (B), deformation is strongly asymmetrical with a detachment shear zone, on one dome limb, and an overhang at the dome base, on the opposite limb (see corresponding total shear strain distribution in figures 2-5 C and D, respectively). The sigmoid shape of the detachment results from the connection, during dome amplification, of the shear zone that accommodates graben opening, at the brittle-ductile interface, with the base middle crust shear zone.*

2.5. Discussion and conclusions

The above preliminary results of thermo-mechanical modeling provide new insights on the development and structure of extensional gneiss domes. At least four main aspects provide matter for discussion. Conclusive remarks are highlighted in italics.

2.5.1. Dynamic inferences

Even if our purpose primarily concerned the analysis of deformation patterns associated with the development of gneiss domes at the crustal scale, our experiments confirm, from a dynamic point of view, a number of conclusions obtained in several previous studies. In particular, they strongly confirm the idea that lower crustal channel flow is necessary, on a scale significantly larger than gneiss domes, to maintain a flat Moho geometry (Block and Royden, 1990; Buck, 1991; Wdowinski and Axen, 1992). Calculations show that *both initial Moho temperature and boundary displacement rate, which directly control middle and lower crust strength, have significant influence on the decrease of Moho depth at regional scale and Moho arching below rising domes, during ongoing extension.* However, it appears that for the tested parameter range, the variations in boundary displacement rate, from 0.66 to 2.0 cm/y, have a stronger influence on Moho response and on the rate of dome amplification than the variations of the initial Moho temperature, (from 840°C to 1040°C). The so-called “core complex mode” introduced by Buck (1991) requires extremely hot geotherms with Moho temperatures of at least 1200°C at 50 km depth. Our models suggest that such hot geotherms are not required. Finally, it must be pointed out that, *even if an increase by a factor of three in boundary displacement rate leads to significant differences in Moho response and rate of dome amplification, the resulting dome geometries and associated strain patterns remain rather similar.* This is likely due to the fact that the growth rate of the doming instability is also controlled by local factors, such as viscosity and buoyancy contrast.

2.5.2. From upper crust necking to dome exhumation

Deformation in the models is characterized by two successive stages. *During the first stage of short duration, a necking instability develops in the upper brittle crust giving rise to a symmetrical graben bounded by conjugate normal faults.* Thinning of brittle crust is responsible for a reduction of the vertical load and consequently a horizontal pressure gradient at depth. This induces a lateral flow of lower crust material toward the zone of necking, initiating a dome. The rather symmetrical pattern of shear zones during the necking stage, suggests that early stages of extension are of approximately pure shear type, at the lithosphere scale. *Extreme thinning and rupture of the upper crust in the graben area then allows middle-lower crust to rise close to the surface. Further dome growth becomes asymmetric with a sigmoid shape detachment zone developing along one dome limb.*

A rather similar process of extensional gneiss dome formation, starting with a symmetrical graben in the upper crust, is also observed in brittle-ductile analogue experiments. (Brun et al., 1994) The experiments, with resolution better than the present numerical models, illustrate how secondary faulting, within an initially symmetrical crustal graben, accommodates extreme asymmetrical brittle crust thinning. In the Aegean, the

Corinth Gulf graben (Armijo et al., 1996; Bernard et al., 1997; Rietbrock et al., 1996) is likely an example of upper crust necking preceding a dome formation (Jolivet, 2001). As proposed by Chéry (2001) in a thought-provocative and stimulating comparison with the Snake Range, the Corinth Gulf steep normal faults may form a low angle décollement at depth.

2.5.3. Crustal-scale detachment

As already pointed out, the origin and mechanics of extensional detachments is a matter of debate. It is however beyond the scope of the present paper to discuss the numerous arguments that accumulated along more than 15 years of field observations, theory and modeling and which mostly concerned the initial flat lying versus steeply dipping attitude of the detachment in the upper brittle crust. Our results may shed light on the development of detachments at the crustal-scale.

Our models show that *extensional detachment zones at crustal scale result from an interaction between faulting, extreme thinning and rupture of the upper brittle crust, and lower crustal flow.* At early stages of development, deformation gives rise to a system of conjugate shear zones, corresponding to a rather symmetrical kinematic pattern, and no detachment is present. With increasing extension, the pattern becomes asymmetric, with the development of a detachment zone.

The detachment develops entirely in the middle crust, whose upper part is progressively exhumed during extension. It results from the connection between a flat-lying shear zone at the graben base that propagates downward, and a basal middle crust shear zone that propagates upward, resulting in a sigmoid shape at the crustal scale. The basal graben shear zone corresponds to ductile deformation close to the brittle-ductile interface, which accommodates brittle stretching within the opening graben. This can be directly compared to the present day deformation below the Corinth Gulf graben (Chéry, 2001). Because the entire detachment identified in our models develops in the ductile middle crust, equivalent structures in the field should be restricted to the mylonitic part of observed detachments. The spatial resolution of our models does not allow a description of the brittle deformation counterpart.

Using the same numerical code as ours, Lavier et al. (1999; 2000) have studied in detail the development of extensional faulting in the brittle upper crust in an ideal two-dimensional brittle layer floating on an inviscid fluid. Multiple major faults with small offset, or a single major fault that can develop very large offset, are obtained depending on the brittle layer thickness for a given cohesion, and the rate of cohesion reduction with strain. A single major fault with large offset and an overall upward convex shape develops for small brittle layer thicknesses and a slow rate of fault weakening. As pointed out by Lavier et al. (1999; 2000), this type of major fault with large offset might compare to some core complex detachment. As demonstrated by the above models and by previous laboratory experiments (Brun et al., 1994), however even a graben type structure can accommodate extreme thinning of brittle upper crust, leading to the exhumation of a gneiss dome capped by a flat lying mylonitic detachment. Field examples of strongly stretched upper crust with conjugate, rotated normal faults lying above mylonitic detachments have been described (Harms and Price, 1983; Miller, 1971; Rehrig, 1986). Such structures are interpreted by Rehrig (1986) as a possible evidence of dominant flattening and co-axial pure shear. We suggest that it could alternatively correspond to the extreme attenuation of grabens above a rising mylonitic detachment. Therefore, *both a single fault with large offset and highly stretched grabens are*

realistic options for brittle crust deformation above a mylonitic detachment. In both cases, faults with initially steep dip are rotated to low angle during extreme extension.

In summary, in our models, detachments associated with extensional gneiss domes form and reach the surface during the course of dome amplification. *No single fault or shear zone cuts up the surface from the onset of extension.*

2.5.4. Comparison with natural examples of gneiss domes

Our dome models show a number of features that can be directly compared with natural examples. Comparison can be made with core complexes and/or gneiss domes from the Basin and Range or the Aegean where erosion has not yet attained deep crustal levels or with extensional gneiss domes from older mountain belts that are more deeply eroded. However, in both cases, only the upper part of the structure displayed by models at the crustal scale can be observed in the field.

The main points of comparison are (1) the overall asymmetry of domes, in particular due to the presence of a detachment fault along one dome limb, (2) the upward convex shape of the detachment, (3) the opposite senses of shear in opposite dome limbs and (3) the strong thinning of middle crust layers. All these characteristics are, for example, observed in gneiss domes of the Aegean (Gautier and Brun, 1994a; Gautier and Brun, 1994b; Gautier et al., 1993). The strong thinning of middle crust layers in the dome limbs and roof reduces the distance between metamorphic isograds, leading to apparent steep temperature gradients. In the Hercynian Montagne Noire Gneiss Dome (the Massif Central, France; (Van Den Driessche and Brun, 1991) where the geotherm calculated from metamorphic parageneses is 37 °C/km (Thompson and Bard, 1982), the apparent gradient reaches 200-300°C/km (Schuilling, 1960) giving mean values of layer perpendicular shortening higher than 75 %.

Models show that the lower crust rises vertically at rather upper crustal levels within dome cores. Evidence of rocks from the base of the middle crust within gneiss domes is commonly found in many gneiss-migmatite domes with pressures in the range 800-1000 MPa (Jones and Brown, 1990; Norlander et al., 2002). There are few examples of domes that exhibit large volumes of lower crust rocks at the surface, such as high pressure granulites. However, the Saxonian Granulite dome of the Bohemian Massif (Reinhardt and Kleemann, 1994), where peak pressures are in the range 1050-1250 MPa, is likely a good example. As described by Reinhardt and Kleemann (1994), the dome, like our models, displays an extensional detachment on one limb and opposite senses of shear along the other limb. Moreover, a component of flattening – i.e., layer perpendicular shortening- up to 50% (Starkey, 1979) or even 70% (Reinhardt and Kleemann, 1994) - is combined with shearing along the dome margins.

The above comparison of models with natural domes should be completed by comparison at the crustal scale, using available deep seismic data. Model predictions concerning structures directly related to lower crustal flow, in particular the dome overhang and the lower upward-concave part of the detachment, represent future challenges in seismic interpretation.

Acknowledgments

C. Tirel acknowledges her thesis grant from the French Ministry of Education and Research. This work is funded by the Institut Universitaire de France grant attributed to Jean-Pierre Brun. E. Burov thanks Y. Podladchikov and A. Poliakov who have co-developed the kernel of PAROVOZ and generously shared their expertise on different stages of its further evolution. Thanks to Muriel Gerbault for discussions and advice on strain plots. We thank Denis Gapais for critical reading of an earlier version of the manuscript, the referees S. Cruden and T. Gerya, and the editor D. Whitney for their remarks and suggestions of improvement.

References

Allmendinger, R.W. et al., 1987. Deep seismic reflection characteristics of the continental crust. Geology, 15: 304-310.

Andersen, T.B., Jamtveit, B., Dewey, J.F. and Swensson, E., 1991. Subduction and eduction of continental crust; major mechanisms during continent-continent collision and orogenic extensional collapse, a model based on the South Norwegian Caledonides. Terra Nova, 3: 303-310.

Armijo, R., Meyer, B., King, G.C.P., Rigo, A. and Papanastassiou, D., 1996. Quaternary evolution of the Corinth Rift and its implications for the Late Cenozoic evolution of the Aegea. Geophys. J. Int., 126: 11-53.

Armijo, R., Tapponnier, P., Mercier, J.L. and Han, T.-L., 1986. Quaternary extension in southern Tibet: field observations and tectonic implications. J. Geophys. Res., 91(B14): 13,803-13,872.

Bernard, P. et al., 1997. The Ms=6,2R June 15 1995 Aigion earthquake (Greece): evidence for low angle normal faulting in Corinth rift. J. Seismol., 1: 131-150.

Berthé, D., Choukroune, P. and Jegouzo, P., 1979. Orthogneiss, mylonites and non-coaxial deformation of granites: the example of the south Armorican Shear Zone. J. Struct. Geol., 11: 31-42.

Bird, P., 1979. Continental delamination and the Colorado Plateau. J. Geophys. Res., 86: 4891-4903.

Block, L. and Royden, L.H., 1990. Core complex geometries and regional scale flow in the lower crust. Tectonics, 9(4): 557-567.

Brace, W.F. and Kohlstedt, D.L., 1980. Limits on Lithospheric Stress Imposed by Laboratory Experiments. J. Geophys. Res., 85(B11): 6248-6252.

Brun, J.-P., Sokoutis, D. and Van Den Driessche, J., 1994. Analogue modeling of detachment fault systems and core complexes. Geology, 22(4): 319-322.

Brun, J.-P., Sokoutis, D. and Van Den Driessche, J., 1995. Analogue modeling of detachment fault systems and core complexes: Reply. Geology, 23(3): 288.

Brun, J.-P. and Van Den Driessche, J., 1994. Extensional gneiss domes and detachment fault systems; structure and kinematics. Bull. Soc. géol. France, 165(6): 519-530.

Buck, W.R., 1988. Flexural rotation of normal faults. Tectonics, 7(5): 959-973.

Buck, W.R., 1991. Modes of continental lithospheric extension. J. Geophys. Res., 96(B12): 20,161-20,178.

Burg, J.P., Brunel, M., Gapais, D., Chen, G.M. and Liu, G.H., 1984. Deformation of leucogranites of the crystalline main central thrust sheet in southern Tibet (China). J. Struct. Geol., 6: 535-542.

Burg, J.P., Van Den Driessche, J. and Brun, J.-P., 1994. Syn to post-thickening extension in the Variscan Belt of Western Europe: Modes and structural consequences. Géologie de la France, 3: 33-51.

Burov, E. and Cloetingh, S., 1997. Erosion and rift dynamics; new thermomechanical aspects of post-rift evolution of extensional basins. Earth Planet. Sci. Lett., 150(1-2): 7-26.

Burov, E. and Poliakov, A., 2001. Erosion and rheology controls on synrift and postrift evolution; verifying old and new ideas using a fully coupled numerical model. J. Geophys. Res., 106(B8): 16,461-16,481.

Chéry, J., 2001. Core complex mechanics: From the Gulf of Corinth to the Snake Range. Geology, 29(5): 439-442.

Coney, P.J. and Harms, T.A., 1984. Cordilleran metamorphic core complexes: Cenozoic extensional relics of Mesozoic compression. Geology, 12: 550-554.

Crittenden, M.D., Coney, P.J. and Davis, G.H. (Editors), 1980. Cordilleran metamorphic core complexes. Geological Society of America Memoir, 153, Boulder, C.O., 1-490 pp.

Cundall, P.A., 1989. Numerical experiments on localization in frictional materials. Ingenieur-Archiv., 59: 148-159.

Cundall, P.A., 1990. Numerical modelling of jointed and faulted rock. In: A. Rossmanith (Editor), Mechanics of jointed and faulted rock. Balkema, Rotterdam, pp. 11-18.

Davis, G.A. and Coney, P.J., 1979. Geological development of metamorphic core complexes. Geology, 7(3): 120-124.

Dewey, J.F., 1988. Extensional collapse of orogens. Tectonics, 7: 1123-1139.

Doin, M.P. and Fleitout, L., 1996. Thermal evolution of the oceanic lithosphere: an alternative view. Earth Planet. Sci. Lett., 142: 121-136.

Echtler, H. and Malavieille, J., 1990. Extensional tectonics, basement uplift and Stephano-Permian collapse basin in a late Variscan metamorphic core complex (Montagne Noire, southern Massif Central). Tectonophysics, 177: 125-138.

England, P.C. and Bickle, M., 1984. Continental thermal and tectonic regimes during the Archaean. J. Geol., 92: 353-367.

England, P.C. and Richardson, S.W., 1977. The influence of erosion upon the mineral facies of rocks from different metamorphic environments. J. Geol. Soc. London, 22: 201-213.

England, P.C. and Thompson, A., 1986. Some thermal and tectonic model for crustal melting in continental collision zones. In: M.P. Cowards and A.C. Ries (Editors), Collision Tectonics. Geological Society Special Publication, London, pp. 83-94.

Gaudemer, Y., Jaupart, C. and Tapponnier, P., 1988. Thermal control on post-orogenic extension in collision belts. Earth Planet. Sci. Lett., 89: 48-62.

Gautier, P., Ballèvre, M., Brun, J.-P. and Jolivet, L., 1990. Extension ductile et bassins sédimentaires mio-pliocènes dans les Cyclades (îles de Naxos et Paros). C. R. Acad. Sci. Paris, 310: 147-153.

Gautier, P. and Brun, J.-P., 1994a. Crustal-scale geometry and kinematics of late-orogenic extension en the central Aegean (Cyclades and Evvia Islands). Tectonophysics, 238: 399-424.

Gautier, P. and Brun, J.-P., 1994b. Ductile crust exhumation and extensional detachments in the central Aegean (Cyclades and Evvia Islands). Geodinamica Acta, 7: 57-85.

Gautier, P., Brun, J.-P. and Jolivet, L., 1993. Structure and kinematics of Upper Cenozoic extensional detachment on Naxos and Paros (Cyclades Islands, Greece). Tectonics, 12: 1180-1194.

Gautier, P. et al., 1999. Timing, kinematics and cause of Aegean extension: a scenario based on a comparison with simple analogue experiments. Tectonophysics, 315: 31-72.

Gerbault, M., Burov, E.B., Poliakov, A.N.B. and Dagnières, M., 1999. Do faults trigger folding in the lithosphere? Geophys. Res. Lett., 26(2): 271-274.

Gerya, T.V., Maresch, W.V., Willner, A.P., Van Reenen, D.D. and Smit, C.A., 2001. Inherent gravitational instability of thickened continental crust regionally developed low- to medium-pressure granulite facies metamorphism. Earth Planet. Sci. Lett., 190: 221-235.

Guillou-Frottier, L., Burov, E.B. and Milési, J.P., 2000. On the genetic links between epithermal ore deposits and ash flow calderas. J. Volcanol. Geotherm. Res., 102(3-4): 339-361.

Harms, T.A. and Price, R.A., 1983. The Newport fault, Eocene crustal stretching, necking and listric normal faulting in northeast Washington and northwest Idaho. Geological Society of America Abstracts with Programs, 15: 309.

Hauser, E. et al., 1987. Crustal structure of eastern Nevada from COCORP deep seismic reflection data. Geol. Soc. Amer. Bull., 99: 833-844.

Herren, E., 1987. Zanskar shear zone: Northeast-southwest extension within the higher Himalayas (Ladakh, India). Geology, 15: 409-413.

Jolivet, L., 2001. A comparison of geodetic and finite strain in the Aegean, geodynamic implications. Earth Planet. Sci. Lett., 187: 95-104.

Jolivet, L. et al., 1998. Midcrustal shear zones in postorogenic extension: Example from the northern Tyrrhenian Sea. J. Geophys. Res., 103(B6): 12,123-12,160.

Jones, K.A. and Brown, M., 1990. High-temperature 'clockwise' P-T paths and melting in the development of regional migmatites: an example from southern Brittany, France. J. Metamorph. Geol., 8: 551-578.

Kirby, S.H. and Kronenberg, A.K., 1987. Rheology of the Lithosphere: Selected Topics. Reviews of Geophysics, 25(6): 1219-1244.

Lavier, L.L., Buck, W.R. and Poliakov, A.N.B., 1999. Self-consistent rolling-hinge model for the evolution of large-offset low-angle normal faults. Geology, 27(12): 1127-1130.

Lavier, L.L., Buck, W.R. and Poliakov, A.N.B., 2000. Factors controlling normal fault offset in an ideal brittle layer. J. Geophys. Res., 105(B10): 23,431-23,442.

Lefort, J.-P. et al., 1987. Crustal generation of the Himalayan leucogranites. Tectonophysics, 134: 39-57.

Lister, G.S. and Baldwin, S.L., 1993. Plutonism and the origin of metamorphic core complexes. Geology, 21: 607-610.

Lister, G.S., Banga, G. and Feenstra, A., 1984. Metamorphic core complexes of Cordilleran type in the Cyclades, Aegean Sea, Greece. Geology, 12: 221-225.

Lister, G.S. and Davis, G.A., 1989. The origin of metamorphic core complexes and detachment faults formed during Tertiary continental extension in the northern Colorado River region, U.S.A. J. Struct. Geol., 11: 65-94.

Makris, J., 1978. The crust and upper mantle of the Aegean region from deep seismic soundings. Tectonophysics, 46: 269-284.

Malavieille, J., Guillot, P., Costa, S., Lardeaux, J.M. and Gardien, V., 1990. Collapse of the thickened Variscan crust in the French Massif Central: Mount Pilat extensional shear zone and St-Etienne late Carboniferous basin. Tectonophysics, 177: 139-149.

McKenzie, D., Nimmo, F., Jackson, J.A., Gans, P.B. and Miller, E.L., 2000. Characteristics and consequences of flow in the lower crust. J. Geophys. Res., 105(B5): 11,029-11,046.

Miller, F.K., 1971. The Newport fault and associated mylonites, northeastern Washington. U.S. Geological Survey Professional Paper, 750D: D77-D79.

Norlander, B.H., Whitney, D.L., Teyssier, C. and Vanderhaeghe, O., 2002. Partial melting and decompression of the Thor-Odin dome, Shuswap metamorphic core complex, Canadian Cordillera. Lithos, 61: 103-125.

Norton, M.G., 1986. Late Caledonides extension in western Norway: a response to extreme crustal thickening. Tectonics, 5: 195-204.

Oldow, J.S., Bally, A.W., Avé Lallemant, H.G. and Leeman, W.P., 1989. Phanerozoic evolution of the North American Cordillera; United States and Canada. In: A.W. Bally and A.R. Palmer (Editors), The Geology of North America--An overview. Geological Society of America, The Geology of North America, Boulder, Colorado, pp. 139-232.

Oxburg, E.R. and Turcotte, D., 1974. Thermal gradients and regional metamorphism in overthrust terrains with special reference to eastern Alps. Schweizerische Mineralogische Petrographische Mitteilungen, 54: 641-662.

Poliakov, A.N.B., Cundall, P., Podlachikov, Y. and Laykhovsky, V., 1993. An explicit inertial method for the simulation of visco-elastic flow: an evaluation of elastic effects on diapiric flow in two and three-layers models. In: D.B. Stone and S.K. Runcorn (Editors), Flow and Creep in the Solar System: Observations, Modelling and Theory, Dynamic Modelling and Flow in the Earth and Planets Series. Kluwer, Holland, pp. 175-195.

Ramberg, H., 1981. Gravity, Deformation and Earth's crust, second edition. Academic Press, London, 452 pp.

Ramsay, J.G., 1967. Folding and fracturing of Rocks, New York, 568 pp.

Ranalli, G., 1997. Rheology of the lithosphere in space and time. In: J.P. Burg and M. Ford (Editors), Orogeny through Time. Geological Society of London Special Publication, London, pp. 19-37.

Ranalli, G. and Murphy, D.C., 1987. Rheological stratification of the lithosphere. Tectonophysics, 132(4): 281-295.

Ratschbacher, L., Frisch, W., Neubauer, F., Schmid, S.M. and Neugebauer, F., 1989. Extension in compressional orogenic belts: the Eastern Alps. Geology, 17: 404-407.

Rehrig, W.A., 1986. Processes of regional Tertiary extension in the western Cordillera: Insights from the metamorphic core complexes. Geol. Soc. Amer. Spe. Publ., 208: 97-122.

Rehrig, W.A. and Reynolds, S.J., 1980. Geologic and geochronologic reconnaissance of a northwest-trending zone of metamorphic core complexes in southern and western Arizona. In: M.C. Crittenden, P.J. Coney and G.H. Davis (Editors), Cordilleran metamorphic core complexes. Gelogical Society of America Memoir, Boulder.

Reinhardt, J. and Kleemann, U., 1994. Extensional unroofing of granulitic lower crust and related low-pressure, high-temperature metamorphism in the Saxonian Granulite Massif, Germany. Tectonophysics, 238: 71-94.

Rey, P., Vanderhaeghe, O. and Teyssier, C., 2001. Gravitational collapse of the continental crust: definition, regimes and modes. Tectonophysics, 342(435-449).

Reynolds, S.J. and Rehrig, W.A., 1980. Mid-Tertiary plutonism and mylonitization, South Mountains, central Arizona. In: M.C. Crittenden, P.J. Coney and G.H. Davis (Editors), Cordilleran metamorphic core complexes. Gelogical Society of America Memoir, Boulder, pp. 159-175.

Rietbrock, A., Tiberi, C., Scerbaum, F. and Lyon-Caen, H., 1996. Seismic slip on a low angle normal fault in the Gulf of Corinth: evidence from high-resolution cluster analysis of microearthquakes. Geophys. Res. Lett., 23: 1817-1820.